Desalination and Water Treatment
www.deswater.com

doi: 10.5004/dwt.2019.24645

168 (2019) 324–339
November

Film-pore diffusion modeling for the adsorption of aqueous dye solution onto acid-treated sugarcane bagasse

Mathivanan Mahalakshmi*, S.E. Saranaathan

School of Civil Engineering, SASTRA Deemed University, Thanjavur 613 402, India, Tel. +91 9488489279/+91 9842673047; emails: mahalakshmi@civil.sastra.edu (M. Mahalakshmi), saranaathan@civil.sastra.edu (S.E. Saranaathan)

Received 31 January 2019; Accepted 29 June 2019

ABSTRACT

The adsorption of methylene blue dye onto acid-treated sugarcane bagasse (ASB) was investigated in batch system. The characterization of ASB was investigated using scanning electron microscopy, X-ray diffractometer and Fourier transform infra-red spectroscopy. The different factors namely adsorbent dosage, solution pH, initial composition of dye solution and temperature on specific dye uptake were examined using ASB in order to evaluate equilibrium kinetic parameters. The suitable variables (dosage = 5 g dm^{-3}; initial pH = 6) for the maximum specific uptake of dye onto ASB. The maximum adsorption capacity of 45.4 mg g^{-1} was obtained at 25°C using ASB. In order to evaluate decay rate and concentration independent mass transfer parameters namely diffusivity and mass transfer co-efficient for adsorption of methylene blue on ASB, the film pore mass transfer model was considered. In this study, external mass transfer co-efficient and pore diffusivity are ranging between 10^{-6} and 10^{-12} m^2 s^{-1}, respectively. The rate limiting step for the adsorption of MB on ASB was known to be internal pore diffusion owing to the higher value of Biot number.

Keywords: Sugarcane bagasse; Kinetic parameters; Pore diffusion model; Methylene blue dye

1. Introduction

Dye removal is a challenging task to protect our surrounding and living organisms [1]. Dye effluent has toxic, mutagenic, non-biodegradable and carcinogenic properties due to the presence of aromatic chemical compounds. Methylene Blue (MB), a cationic dye, potentially employed for coloring the cotton, wool and silk stuffs due its good adsorption capability in various dyeing industries. The following toxic effects were so far reported due to the discharge of MB-containing textile effluent. (i) gastritis, (ii) eye irritation, (iii) breathing difficulties, (iv) nausea, (v) vomiting, (vi) tissue necrosis, (vii) cyanosis, (viii) painful micturition, (ix) mental confusion and (x) methemoglobinemia. However, MB is effectively employed in the medical field for curing Nile virus, psoriasis and Duck hepatitis B diseases [2,3]. A very low concentration of dye and its degradation product can cause high disorders to human beings. The treatment of dye effluent by biological methods was proposed by metabolic activity of enzyme secreted from microbes during fermentation. However, it has certain limitations of microbial contamination and formation of toxic and carcinogenic intermediate from dye degradation process during solid-state fermentation. During anaerobic microbial dye degradation process, water soluble dye substances are transformed to aromatic amine groups by breaking up of azo groups. The formed aromatic amine groups are of high toxic nature than its original form. Due to long treatment time and minimum color removal, dye decolorization by microbial method has certain limitations.

There are various methods namely physical (sedimentation, coagulation, flocculation, membrane technology,

* Corresponding author.

adsorption), chemical (electrochemical oxidation, electrocoagulation, sono-chemical method, photochemical method, ozonation) and biological (aerobic, anaerobic) proposed for the treatment of textile effluent. Owing to low cost, high degree of pollutant removal, absence of sludge formation and simple in nature, adsorption is a potential treatment method than biological and chemical methods [4–9]. Nowadays, the treatment of toxic dye solution by adsorption using lignocellulosic feed stock has been attracted by many researchers due to easy availability, cost effective and sufficient biomass availability. Among the various methods proposed for the treatment of color removal, adsorption significantly reduces the capital cost and operating cost [10–12]. The influencing factors including dosage, pH variation, dye concentration and thermodynamic study on the adsorption of methylene blue dye onto corncob was investigated [13]. There are numerous adsorbents namely fly ash, oil palm frond, *Melia azedarach* sawdust, grated copra, alkali-treated dried sun flower hull, activated carbon, polypyrrole coated sawdust, organo-rice straw, jack fruit leak powder, bengal gram fruit shell and treated fly ash were effectively used for the removal of color in various effluents [14–23]. In the recent past, there are various strategies involved for enhancing adsorption capacity either by modification of adsorbent or treatment of adsorbent. The pretreatment includes steam activation, acid treatment, alkali treatment [24,25], calcium chloride treatment [26]. The treated adsorbent causes rough, enough pore size and cavities which offers large surface area for the easy attachment of dye. Sugarcane bagasse is a solid wasted disposed from fruit juice shop and does not contain any significant commercial value.

To best of our knowledge, the use of treated sugarcane bagasse as adsorbent for the adsorption of MB has not been investigated so far. The present study is focused on the adsorption of dye from aqueous solution on acid-treated sugarcane bagasse (ASB). The effect of different parameters namely quantity of adsorbent, initial pH, initial composition of dye solution and temperature on specific dye uptake was examined. Adsorption kinetic model and film-pore mass transfer model were employed to determine the maximum adsorption capacity and mass transfer parameters namely diffusion co-efficient and external film transfer co-efficient in batch adsorption system.

2. Materials and methods

2.1. Preparation of adsorbent and adsorbate

Sugarcane bagasse obtained from local sugarcane juice shop, Thanjavur, India, was washed with double distilled water, autoclaved at 121°C for 20 min and dried in a hot air oven at 60°C for 2 d. In acid treatment, the collected sugarcane bagasse was autoclaved and soaked into H_2SO_4 (2 N) for 1 h. Then it was rinsed with distilled water till the solution pH reached neutral. Then ASB was dried in hot air oven at 60°C for 2 d. The dried material was subjected to grinding to make fine powder, sieved and BSS−14 + 36 mesh size adsorbent particles were taken and used in further studies. The adsorbate was procured from Ranbaxy Laboratory Limited, India. The characteristics of MB dye solution is as follows: class: cationic thiazine dye; chemical formula: $C_{16}H_{18}N_3SCl$; color index number: 52015; molecular weight: 319.85 g mol^{-1}; color index name: Basic Blue 9 and maximum wavelength: 664 nm.

2.2. Batch adsorption experiment

Dye effluent (100 mL) was taken to 250 mL conical flask, in which suitable dosage of ASB was added. It was kept in orbital shaker at 100 rpm. The sample was withdrawn at appropriate time and filtered. The composition of MB in dye solution was determined by UV–Vis spectrophotometer (Systronics 2201) using 662 nm as a maximum wavelength.

2.3. Evaluation of zero point charge (pH_{PZC})

The point of zero charge (pH_{PZC}) is the one in which the electrical charge density is zero on surface of adsorbent. The effect of initial pH on adsorption of dye on ASB was performed by varying pH (0.1 N H_2SO_4 or 0.1 N NaOH) and also final pH of the solution (pH_f) was determined after equilibrium has been established. After measuring pH_f, the difference between the initial and final pH of the solution ($\Delta pH = pH_i - pH_f$) was plotted with respect to initial pH to determine the zero point pH of derived adsorbent [7].

2.4. Characterization of adsorbent

The Fourier transform infrared spectroscopy (FTIR) analysis of ASB and dye biosorbed on ASB was performed using spectrum RX I, PERKINELMER Spectrum with wave number ranging from 4,000 to 400 cm^{-1}. The nature and surface morphology of adsorbent (treated and untreated) was characterized by powder X-ray diffraction (Rigaku Ultima III XRD) and scanning electron microscopy (VEGA3 TESCAN, SEM), respectively.

2.5. Factors affecting adsorption process using acid-treated adsorbent

The different factors such as dosage, initial pH, initial dye concentration, temperature on specific uptake rate were studied using ASB. The influence of temperature on maximum dye uptake rate was determined. Finally, the feasibility of adsorption was explained by thermodynamic parameters.

2.6. Pore diffusion model

2.6.1. Diffusion-based model

Internal and external mass transfer effects are essential steps to understand the pore diffusion and external mass transfer limitations. The simple mass transfer models are available to determine external mass transfer co-efficient. These models are briefly discussed below.

2.6.2. External film resistance

In the initial stages of adsorption, the external mass transfer limitation is predominant leading to control the rate of adsorption. Therefore, a simplest mass transfer model could be proposed to explain the rate of diffusion by taking material balance across the batch adsorption system. The following

assumptions were considered for the development of external convective mass transfer model:

- The adsorbent particles are in spherical shape.
- The bulk composition of liquid medium surrounding the adsorbent particle is uniform throughout the system due to perfect back mixing.
- Owing to negligible composition in solid phase, the pore diffusion resistance is negligible in the initial stage of adsorption.
- The transfer of solute from the liquid phase is exactly balanced by the total mass transfer rate of solute on the surface of solid particle from the surrounding liquid phase during adsorption.
- The first order rate equation is considered.

The rate of transfer of solute during adsorption is given by

$$\frac{dS}{dt} = -k_s \frac{A_s}{V}\left(S - S_s\right) \tag{1}$$

The mass transfer area per unit volume of the bulk solution is defined as

$$\frac{A_s}{V} = \frac{6M_s}{D_p \rho_b} \tag{2}$$

Integration of Eq. (2) and applying boundary conditions

$$\ln\frac{S_t}{S_0} = -k_s \frac{A_s}{V} t \tag{3}$$

Mass transfer co-efficient (k_s) could be evaluated by Eq. (3).

2.6.3. Two resistance models

If more than one step is involved in the determination of rate controlling, simultaneous partial differential equations (PDEs) were used for batch adsorption system. The following assumptions were considered for the development of mass transfer model:

- The transfer of solute through liquid film over the solid particle.
- The local liquid phase composition is in equilibrium with surface composition on solid particle under isothermal condition.
- Transfer of solute from the external surface of solid particle to interior space occurs due to either one or more of the following mass transfer limitations:
  - Internal pore diffusion [27]
  - Surface diffusion, that is, homogenous surface diffusion model [28] or concentration dependent surface diffusion model
  - Combined diffusion
  - Branched pore diffusion model

The analytical solutions are not applicable for the solution of simultaneous PDEs involved in the model. Therefore, these model equations are solved by Crank–Nicholson implicit finite differential method [29,30]. In this study, film-pore diffusion model has been proposed to describe diffusion rate of MB onto ASB as adsorbent.

Pore diffusion model including both internal pore diffusion and external film resistance significantly plays a major role for controlling rate of mass transfer.

2.7. External mass transfer

The diffusion rate of solute (dye, S_t) through liquid film over the adsorbent surface is directly proportional to change in solute concentration difference

$$\frac{dS_t}{dt} = -k_s \frac{A_s}{V}\left(S_t - S_s\right) \tag{4}$$

2.7.1. Pore diffusion

The internal pore diffusion is described by Fick's law. The mass balance equation for rate of diffusion of solute during pore diffusion in a spherical particle is written by equation as follows:

$$\varepsilon\frac{\partial S_i}{\partial t} + \rho_p \frac{\partial Q_i}{\partial t} = D_e\left[\frac{\partial^2 S_i}{\partial r^2} + \frac{1}{r}\frac{\partial S_i}{\partial r}\right] \tag{5}$$

The boundary conditions are as follows:

$$S_i = 0 \quad \text{for } 0 \le r \le R; \quad \text{when } t = 0 \tag{6}$$

Apply symmetry boundary condition at the centre of solid adsorbent:

$$\frac{\partial S_i}{\partial r} = 0 \text{ at } r = 0 \tag{7}$$

The rate of diffusion of solute through external film on solid particle is exactly balanced by rate of removal of solute from external surface of the adsorbent. Therefore, the second boundary condition (B.C-2) at the outer surface area of the solid particle becomes:

$$k_s(S_t - S_s) = D_e \left.\frac{\partial S_i}{\partial r}\right|_{r=R} \tag{8}$$

2.7.2. Equilibrium

It is assumed that spontaneous equilibrium exists inside the solid particles. Therefore, the concentration of solute on surface of solid particle at any radial direction and time (t) could be associated with solute concentration in liquid phase using the following isotherm expression:

$$Q_i = f(S_i) \tag{9}$$

Now, applying Eq. (9) in Eq. (13)

$$\varepsilon\frac{\partial S_i}{\partial t}+\rho_p\frac{\partial f\left(S_i\right)}{\partial t}=D_e\left[\frac{\partial^2 S_i}{\partial r^2}+\frac{1}{r}\frac{\partial S_i}{\partial r}\right] \tag{10}$$

Langmuir adsorption isotherm is given by

$$Q_i=f\left(S_i\right)=\frac{Q_e K_L S_i}{1+K_L S_i} \tag{11}$$

The mean concentration of solute in the solid phase is expressed as follows:

$$Q_{\text{ave}}=\frac{\int_0^R Qr^2dr}{\int_0^R r^2dr} \tag{12}$$

2.8. Overall material balance

The overall solute balance is written for whole adsorption system with aqueous phase concentration:

$$V\frac{dS_t}{dt}=m_s\frac{dQ_{\text{avg}}}{dt} \tag{13}$$

Apply initial boundary condition:

$$\text{At } t=0,\ S_t=S_0 \text{ and } Q_{\text{avg}}=0 \tag{14}$$

2.9. Dimensionless equations

The following dimensionless parameters were introduced to covert the PDEs to dimensionless forms

$$Z=\frac{r}{R};\quad \overline{S_i}=\frac{S_i}{S_0};\quad \overline{S_t}=\frac{S_t}{S_0};\quad B_i=\frac{k_s R}{D_e};\Bigg\} \tag{15}$$

Eq. (10) can be written as follows:

$$\frac{\partial\overline{S_i}}{\partial\tau}=A\left(\overline{S_i}\right)\left[\frac{\partial^2\overline{S_i}}{\partial Z^2}+\frac{1}{Z}\frac{\partial\overline{S_i}}{\partial Z}\right] \tag{16}$$

where

$$A\left(\overline{S_i}\right)=\frac{1}{\left\{\varepsilon_P+\left(\frac{Q_h\rho_p}{S_0}\right)\left(\frac{1+bS_0}{\left(1+bS_0\overline{S_i}\right)^2}\right)\right\}} \tag{17}$$

The modified boundary conditions in the form of dimensionless are as follows:

$$\overline{S_i}\Big|_{\tau=0}=0\quad \text{for } 0\le Z\le 1 \tag{18}$$

$$\left.\frac{\partial\overline{S_i}}{\partial\tau}\right|_{Z=0}=0,\quad \text{for } \tau\ge 0 \tag{19}$$

$$\text{Bi}(\overline{S_t}-\overline{S_s})=\left.\frac{\partial\overline{S_i}}{\partial Z}\right|_{Z=1} \tag{20}$$

The average concentration of solute in the solid phase is expressed by dimensionless form of integral expression as follows:

$$\overline{Q_{\text{ave}}}=3\int_0^1\overline{Q}Z^2dZ \tag{21}$$

The overall material balance with respect to solute becomes:

$$\frac{d\overline{S_t}}{d\tau}=\frac{m_s Q_h}{VS_{b0}}\frac{d\overline{Q_{\text{avg}}}}{d\tau} \tag{22}$$

Corresponding initial conditions are:

$$\overline{S_t}\Big|_{\tau=0}=\overline{S_0}\qquad \overline{Q_{\text{avg}}}\Big|_{\tau=0}=0 \tag{23}$$

Using method of lines, Eqs. (16)–(23) are solved numerically as described in the following section.

3. Result and discussion

3.1. Characteristics of adsorbent

The surface morphology of the untreated and ASB was examined using the SEM with the magnifications of 5 and 1 kx, respectively, in Fig. 1. The structure of the ASB has rough, irregular size of large pores and cavities which offers large surface area for the easy adsorption of dye molecules than untreated sugarcane bagasse (UASB) powder.

Fig. 2 illustrates the powder XRD pattern of untreated and ASB powder. The XRD pattern of ASB posses two intensity peaks at 2θ nearly at 16.12° and 22.34° in Fig. 2b. The plane of cellulose in the ASB observed with highest intensity peak at 2θ of 22.34°. The weaker intensity peak obtained at 2θ of 16.34° was due to the presence of hemicelluloses and lignin content in the adsorbent, which characters amorphous nature of ligno-cellulosic adsorbent [31]. There is no significant variation in XRD pattern obtained for UASB. Based on the characterization namely surface morphology and XRD pattern, ASB powder was considered in the further studies.

Owing to the availability of cellulose, hemicelluloses and lignin content in the ASB powder, the diverse functional groups including ketone, hydroxyl, sulfydryl, carboxyl, sulfhydryl and aldehydes were present on the surface of adsorbent. The FTIR spectrum is used to examine such characteristic functional groups on the surface of the ASB before and after adsorption. The FTIR spectra of ASB powder illustrated in Fig. 3 describe the several peaks corresponding to the multiple functional groups present of the adsorbent surface. Fig. 3b shows the FTIR spectra of MB adsorbed on ASB powder.

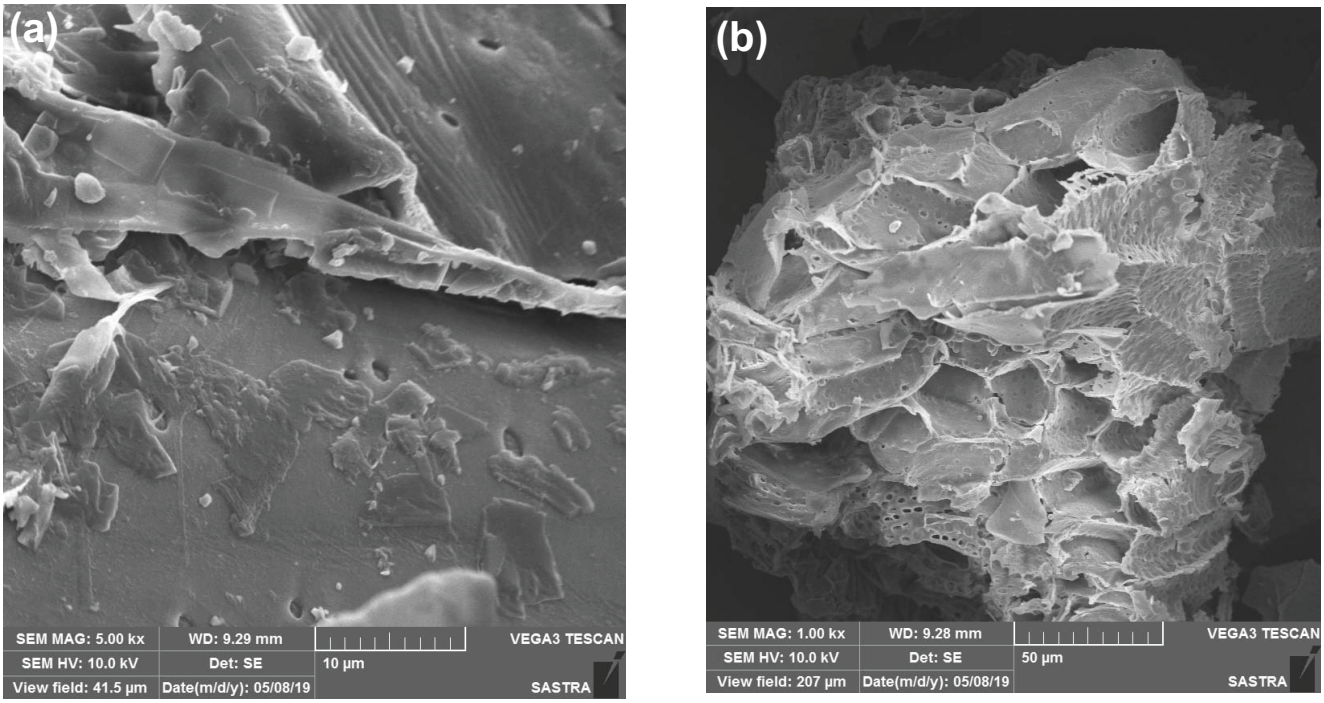

Fig. 1. Surface morphology of sugarcane bagasse powder (a) untreated and (b) treated.

In Fig. 3a the broad absorption peak between 3,400 and 3,000 cm^{-1} described hydroxyl (–OH) stretching vibrations due to the presence of more number of phenolic and alcoholic hydroxyl functional groups [7,32]. The absorption peak observed at 2,922 cm^{-1} indicates the characteristic of the asymmetric and symmetric –CH stretching from lignin content in ASB. A small hump appeared nearly at 1,686 cm^{-1} indicating carbonyl stretching from quinones and lactones [7]. A band obtained at 1,607 cm^{-1} was due to the occurrence of carbonyl groups from the stretching of peptide linkage containing amide-I band [33]. The characteristic peak obtained at 1,415 cm^{-1} describes the presence of carboxylate functional group (–COO) in the adsorbent [7]. The peak appeared at 1,312 cm^{-1} describing the vibration of C–N stretching in the adsorbent. The transmission intensity peak at 1,253 cm^{-1} explained the bending of following groups namely C–C–H, C–O–H and O–C–H on the surface of adsorbent [7]. A strong transmittance at 1,026 cm^{-1} characterizes C–O–C functional group due to the ligno-cellulosic nature of ASB containing lignin, cellulose and hemicelluloses [7].

Fig. 3b describes the FTIR spectra of dye adsorbed on ASB. A minor variation in absorption peak for the stretching vibration of –OH groups was obtained nearly at 3,246 cm^{-1} for the adsorption of MB on ASB. The carbonyl functional group (–C=O) stretching of amide-I band at 1,607 cm^{-1} of ASB was appreciably changed to 1,596 cm^{-1} in the MB adsorbed on ASB. A change in transmittance peak of functional group region of C–N stretching vibrations was noticed at 1,290 cm^{-1}. A minor change in bending vibrations of O–C–H, C–C–H and C–O–H was obtained in MB-loaded ASB. A significant change in absorption peak was identified at 1,036 cm^{-1} for MB loaded on ASB which was originally at 1,026 cm^{-1} of ASB before adsorption.

3.1.1. Effect of dosage of adsorbent dosage on specific dye uptake

The influence of dosage on specific uptake rate of dye onto ASB is shown in Fig. 4. It is shown that specific uptake of dye was decreased as increase in dosage. It is meant that the amount of dye adsorbed over the surface of the adsorbent increases, however the adsorption capacity, the quantity of dye adsorbed per unit amount of the adsorbent decreases by increasing the adsorbent dose. It is meant that increasing the dosage of adsorbent increases the number of active sites available for adsorbing more quantity dye [34,35]. At high dosage of adsorbent, the specific dye uptake was found to be decreased owing to unsaturated adsorption sites with fixed concentration of dye. The aggregation of adsorbent causes the reduction in total surface area of adsorbent and increase in mass transfer limitations [7,36]. The initial adsorption rate of dye is the product of square of specific uptake rate of dye under equilibrium and pseudo-second-order rate constant [37]. Based on the initial rate of adsorption of dye onto ASB, adsorbent dosage (5 g dm^{-3}) was selected and used in further studies.

3.1.2. Effect of pH on specific dye uptake

The difference between initial and final pH of the aqueous dye solution was examined and shown in Fig. 5. Fig. 6 depicts the variation of equilibrium dye uptake rate and final pH with respect to initial pH. The pH_{pzc} value for ASB was found to be 5.

The initial pH of the aqueous dye solution is a crucial factor influencing adsorption, since it affects the ionic strength over the adsorbent surface and ionization potential

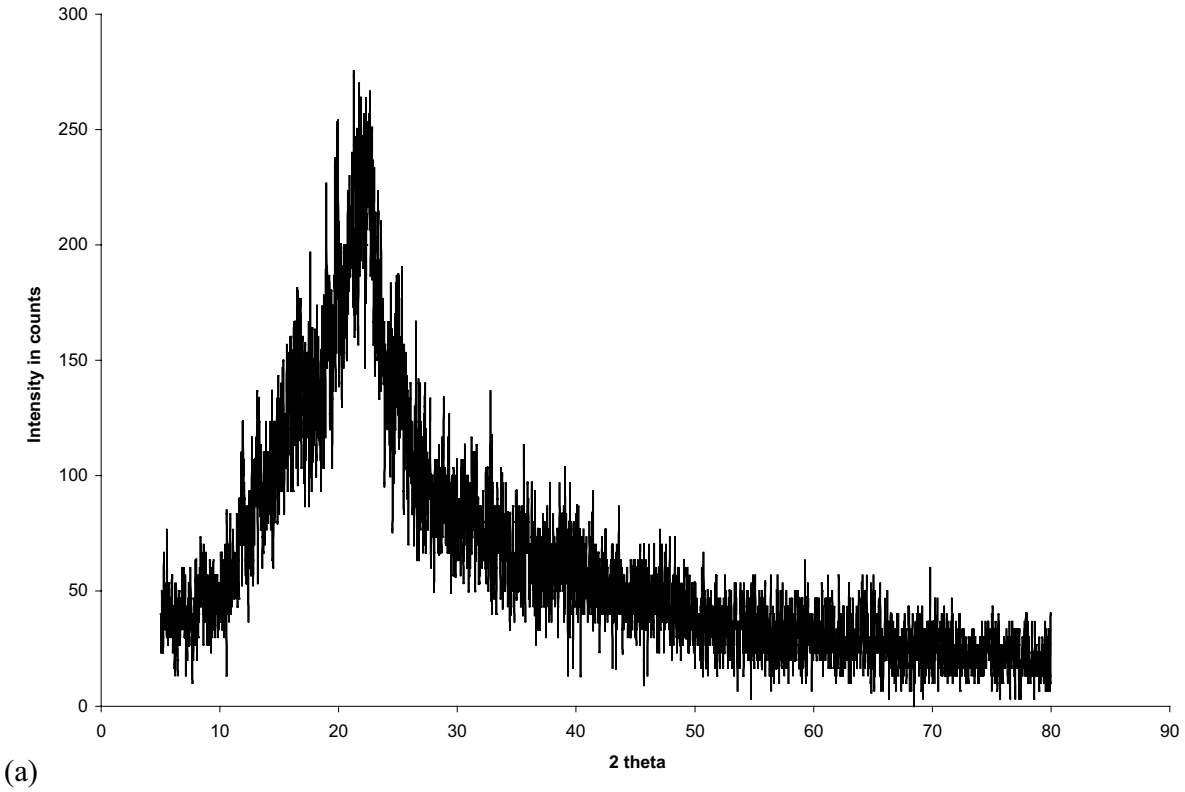

(a)

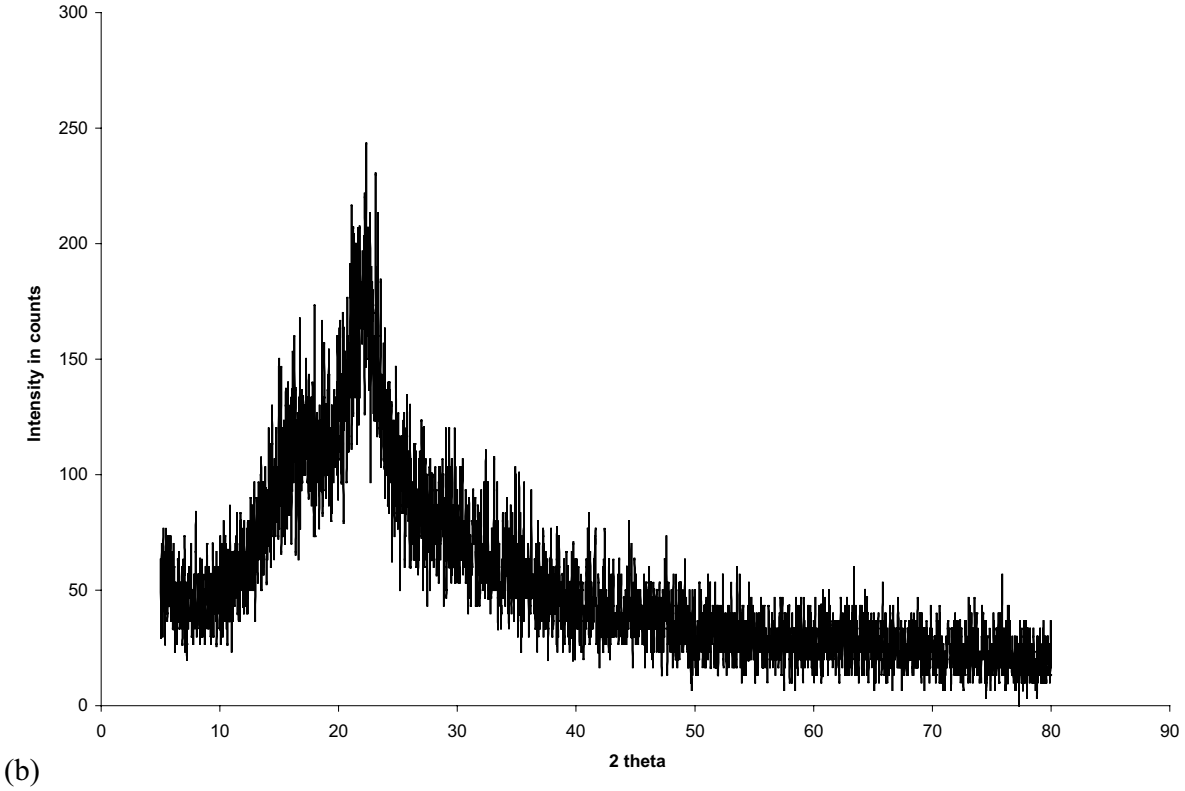

(b)

Fig. 2. XRD pattern for sugarcane bagasse powder (a) untreated and (b) treated.

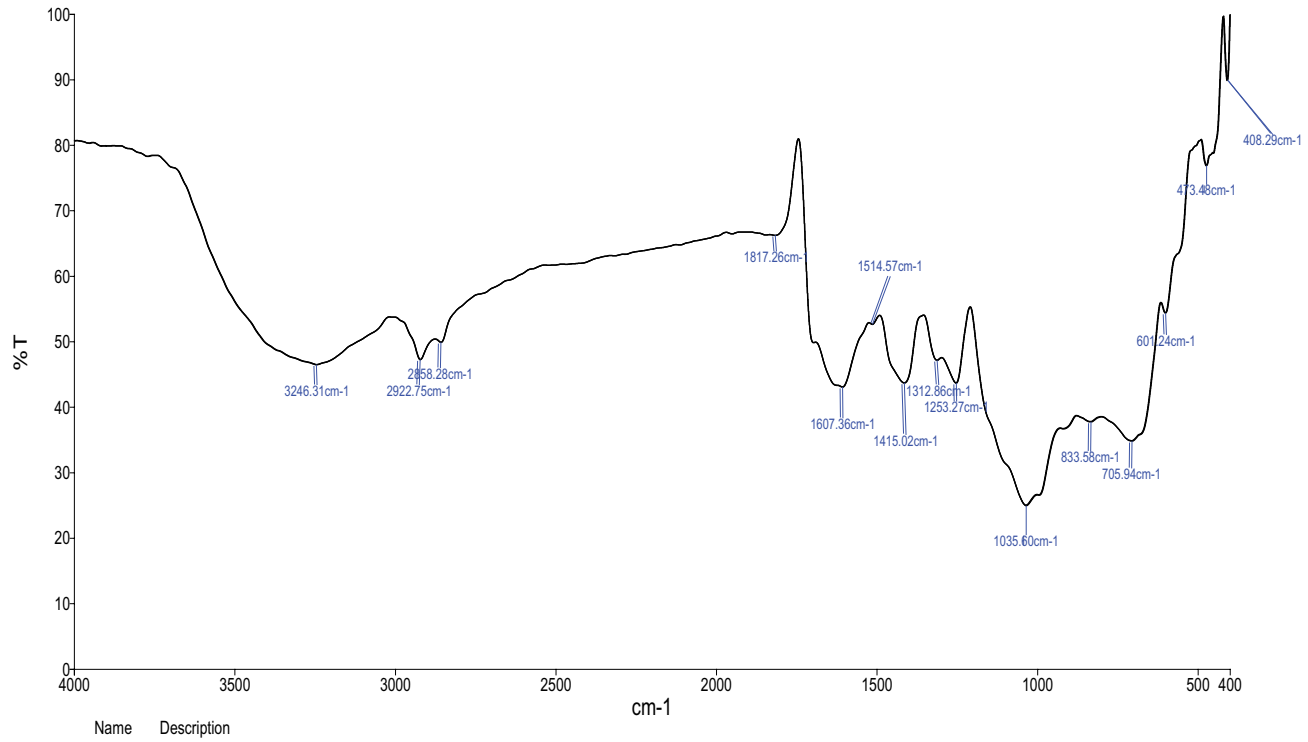

(a)

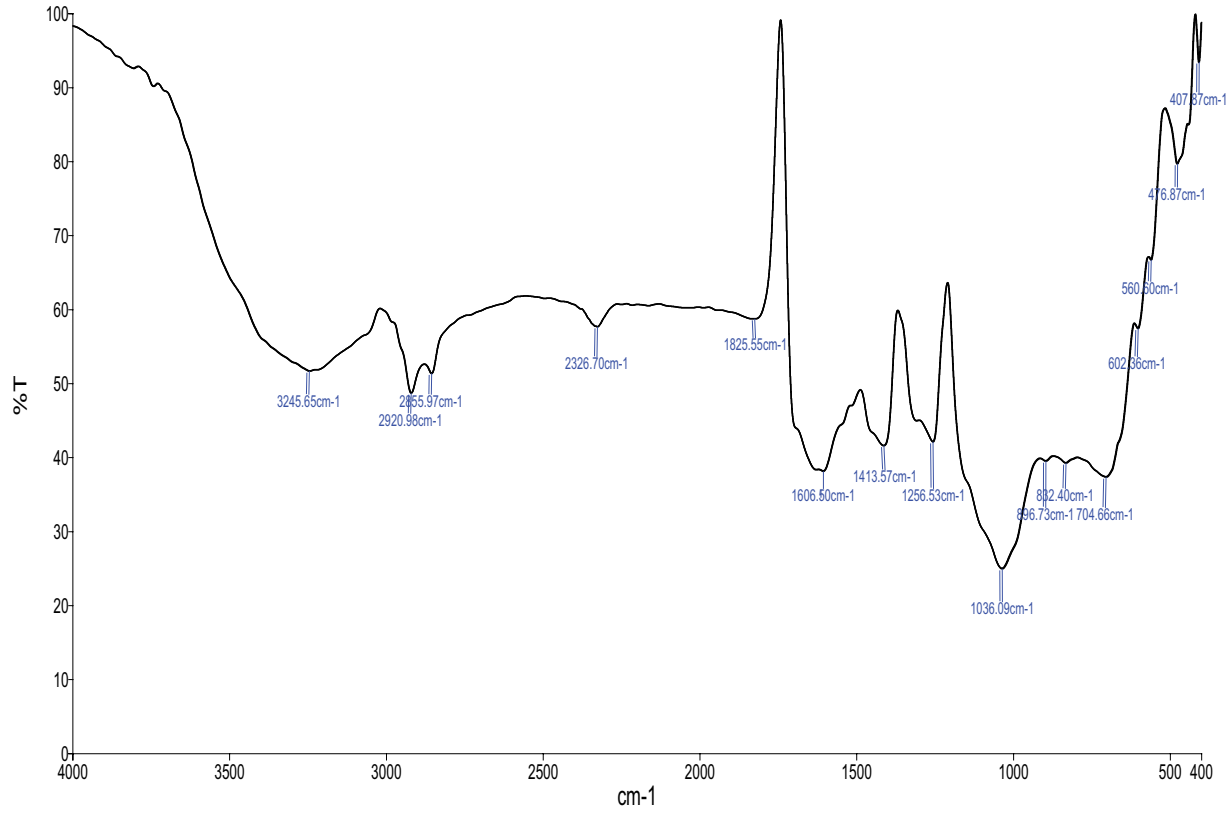

(b)

Fig. 3. FTIR spectra for (a) ASB and (b) Methylen Blue adsorbed on ASB.

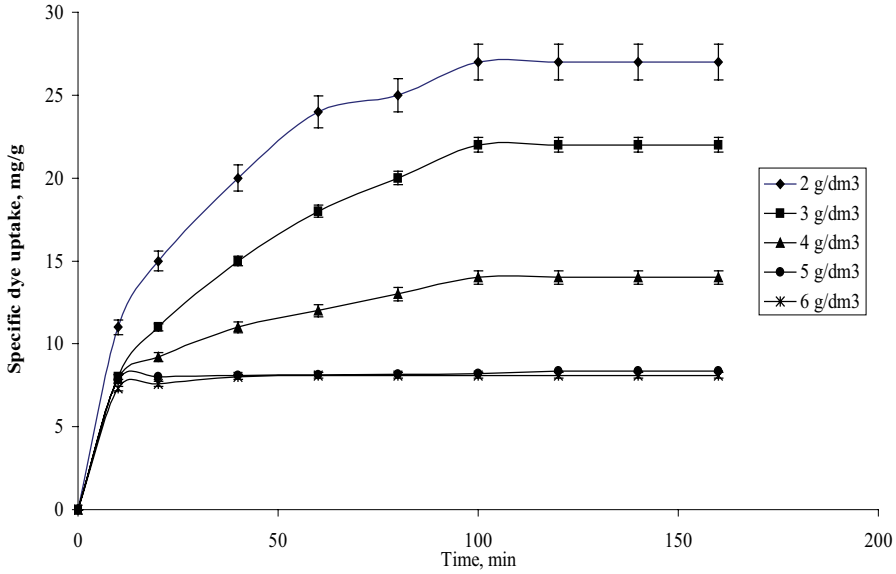

Fig. 4. Effect of dosage on specific uptake of dye onto ASB (initial concentration = 100 mg dm^{-3}; temperature = 303 K; agitation speed = 100 rpm; particle size: BSS ≠ –14 + 36).

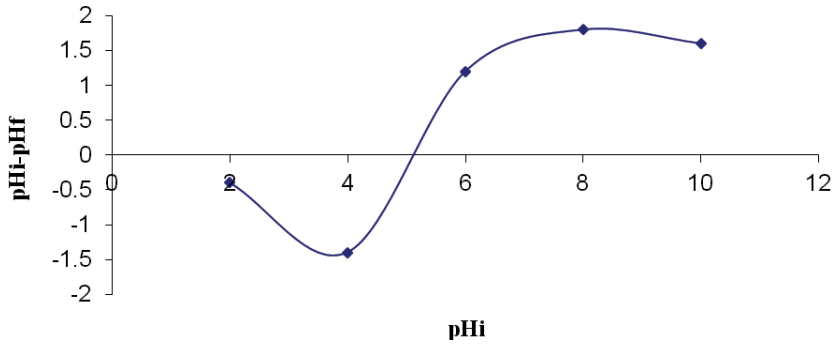

Fig. 5. Effect of initial pH on pH_{pzc} (dosage = 5 g dm^{-3}, agitation speed = 100 rpm; particle size: BSS ≠ –14 + 36).

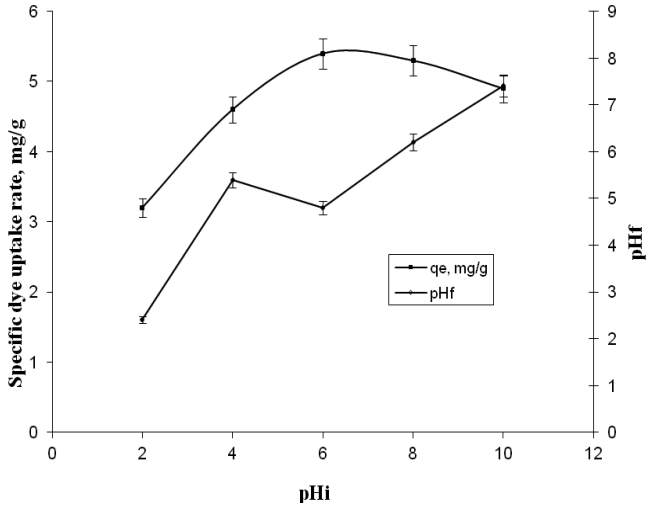

Fig. 6. Effect of initial pH on final pH and equilibrium uptake rate of dye on treated sugarcane bagasse (dosage = 5 g dm^{-3}, agitation speed = 100 rpm; particle size: BSS ≠ –14 + 36).

of adsorbate [7]. The influence of initial pH on specific dye uptake was investigated using ASB with initial dye concentration of 100 mg dm^{-3} and dosage of 5 mg dm^{-3} in the pH ranging from 2 to 10. While increasing the pH of the solution, the specific dye uptake is significantly increased from 3.2 to 5.6 mg g^{-1} and then slowly decreased to 4.8 mg g^{-1}. For the adsorption of MB onto ASB, the maximum specific uptake of dye was attained at the initial solution pH of 6. Generally, the functional groups namely hydroxyl ($–OH^-$), carbonyl ($–C=O^-$), carboxylic ($–COOH_2^+$), phenolic ($–OH_2^-$) and amino ($–NH_2$) distributed on the surface of biosorbate are greatly influenced by varying initial pH [7,34,38,39]. As the pH of the solution decreases lower than pH_{pzc}, the adsorption capacity was found to be decreasing owing to the generation of more number of protons (H^+ ions) in the bulk solution, that is, below the pH_{pzc} value, the surface of adsorbent is protonated and positively charged favoring the attraction of anionic (negative charge) dye using electrostatic force. Conversely, at the high pH level (above pH_{pzc}), the formation of OH^- ions are predominant. Therefore, at the high pH, the adsorption capacity was significantly improved due to the

cationic nature of the dye. The findings are similar to existing reports [40–44]. The following mechanism is proposed for the adsorption of MB onto ASB in the high pH range more than pH_{pzc}:

$$ASB\text{-}OH + OH^- \rightarrow ASB\text{-}O^- + H_2O$$

$$ASB\text{-}O^- + MB\ (cationic) \rightarrow ASB\text{-}O\text{-}\ MB$$

3.1.3. Effect of initial concentration of dye on specific uptake

In order to examine the equilibrium kinetic parameters, the influence of initial concentration of dye on specific uptake of dye was investigated from 50 to 250 mg dm^{-3} with adsorption dosage of 5 g dm^{-3} at different temperature ranging from 25°C to 50°C (Fig. 7).

The experimental results were well in agreement with pseudo-second-order kinetic model with $R^2 > 0.99$. The kinetic parameters for the adsorption of MB onto ASB with different initial concentration of dye solution are listed in Table 1. Initially, the value of specific dye uptake is increased with respect to time until equilibrium is achieved. An increase in dye concentration increases an equilibrium specific dye uptake, where as the value of rate constant is decreased. It might be due to the minimum competition between the dye molecules on the active site of adsorbent in the low concentration of dye solution. The availability of dye solute near the active site for adsorption is huge at high initial dye concentrations which leads to the competition between the dye solutes on adsorption sites, influencing the adsorption capacity of adsorbent. At high initial dye concentration, there may be a chance of insufficient active sites for the adsorption of more number of dye solute molecules [45–47]. Therefore, the increase in specific dye uptake and decrease in second-order rate constant at each temperature was observed by increase in dye concentration. The findings were well in agreement with existing findings [48–51].

3.1.4. Equilibrium adsorption isotherm model

Fig. 8 explains the adsorption isotherm models for the adsorption of MB solution onto ASB as substrate using adsorption models. Langmuir and Freundlich isothermal model parameters are listed in Table 2. It is found that maximum uptake of dye was decreased as increase in temperature from 25°C to 50°C. The maximum uptake of dye (45.4 mg g^{-1}) was obtained at 25°C. As per the value of dimensionless parameter (R_L), adsorption is feasible. The maximum uptake of dye on ASB is compared with existing reports.

It is found that maximum specific adsorption capacity and Freundlich adsorption constant decreased as system temperature increased from 25°C to 50°C. The maximum

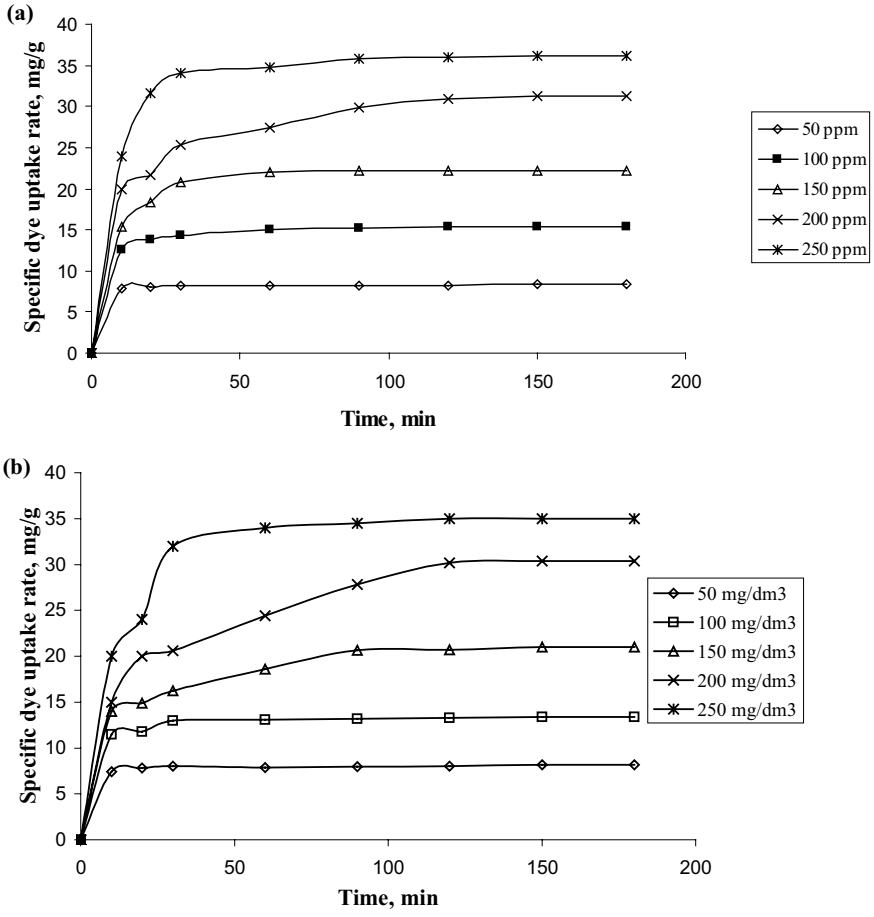

Fig. 7. (*Continued*)

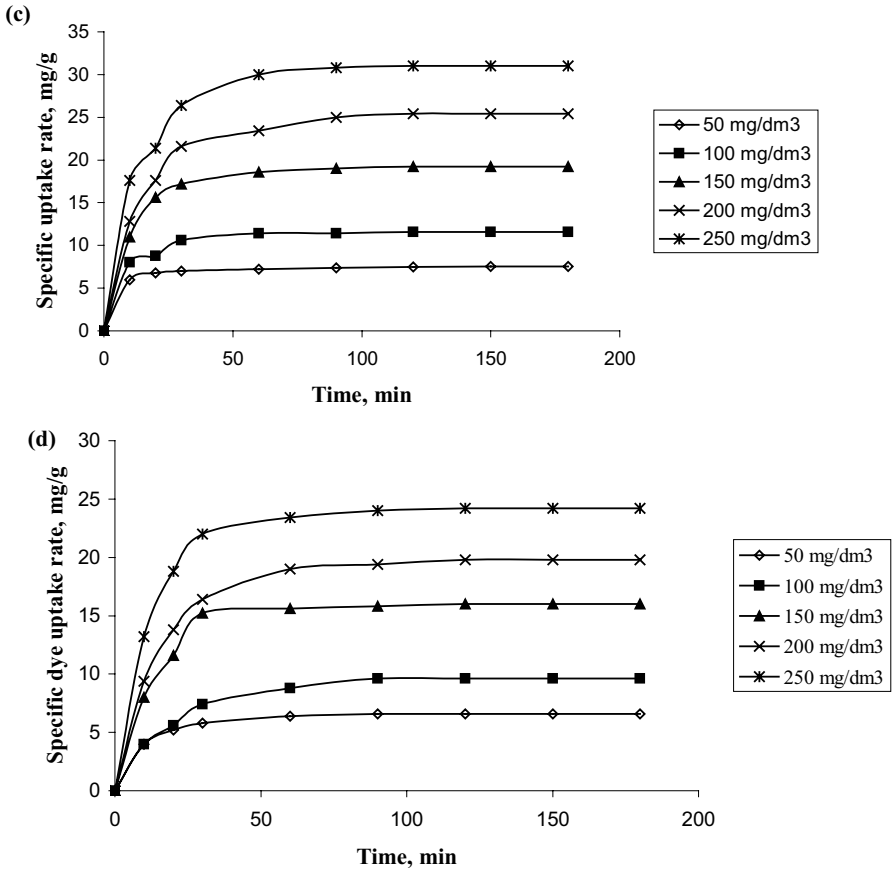

Fig. 7. Effect of initial concentration on adsorption of dye onto ASB (dosage = 5 g dm^{-3}; agitation speed = 100 rpm; particle size: BSS ≠ –14 + 36). (a) Temperature = 25°C, (b) temperature = 30°C, (c) temperature = 40°C and (d) temperature = 50°C.

uptake of dye (45.9 mg g^{-1}) was obtained at 25°C. The separation factor, R_L, indicates the feasibility of adsorption process. In all the experiments, separation factor value was ranging from 0.859 to 0.97 (lower than unity) which explains favorable adsorption process [52]. The equilibrium isotherm constants for the adsorption of MB solution onto ASB are listed in Table 2.

So far, the different cost-effective adsorbents were employed to decolorize the MB dye from aqueous solution. Table 3 represents a comparison of monolayer maximum adsorption capacity of sugarcane bagasse with existing reports. It is clear that the dye adsorption capacity of ASB is comparable.

3.2. Thermodynamic approach

The influence of temperature on equilibrium constant was described by Van't Hoff equation. Thermodynamic parameters namely change in enthalpy (ΔH) and change in entropy (ΔS) were determined from slope and intercept of change in Gibb's free energy (ΔG) using ln$K$ vs. ($1/T$) diagram. The change in Gibb's free energy (ΔG) was determined by Gibb's free energy work function at corresponding system temperature. Thermodynamic properties and specific dye uptake rate were listed out in Table 4. The specific uptake rate of dye on ASB is decreased with increase in system temperature.

The adsorption of dye onto treated SB is not thermodynamically feasible at high temperature range (>40°C) due to the positive (+) value of Gibb's free energy change (ΔG) and negative value of entropy change (ΔS). And also, the negative value of enthalpy change (ΔH) explained exothermic adsorption. The negative (–) value of entropy change (ΔS) confirmed that increased randomness of solute molecule from solid surface to bulk liquid. Therefore, temperature of the system more than 30°C facilitates de-sorption of dye molecules from solid phase. The positive value of entropy change may lead to the removal of water molecules other than solute (dye) from surfaces of various adsorbents during adsorption.

3.3. Determination of mass transfer parameters

3.3.1. Numerical solution

Non-linear adsorption model from Eqs. (16)–(23) was solved by method of lines. The governing PDEs and the boundary conditions were converted into first-order ordinary differential equations (ODEs). The radial derivatives were discretized by central finite difference method. The radius of the solid particle was split into N sections with equal length of $\Delta Z = (N-1)^{-1}$.

The grid points are indexed as $i = 1, 2, 3, 4 \ldots N$; where, $i = 1$ and $i = M$ refer to the center point and external surface

of the particle, respectively. The obtained equation corresponding to the center of adsorbent (solid particle) was derived with the help of L'Hopital's rule to boundary conditions. Equation corresponding to the exterior surface was derived by introducing a false boundary point (N + 1). The fictitious point is removed from this equation by discretized boundary condition at Z = 1. The resulting ODEs are given below:

- At the center (Z = 0, i = 1):

$$\frac{d\overline{S_1}}{d\tau} = 6A\left(\overline{S_1}\right)\left[\frac{\overline{S_2} - \overline{S_1}}{\Delta Z}\right] \tag{24}$$

- At the interior points (i = 2, 3, 4, …. N–1)

$$\frac{d\overline{S_i}}{d\tau} = \frac{A\left(\overline{S_i}\right)}{\Delta Z^2}\left[\left(\overline{S_{i+1}} - 2\overline{S_i} + \overline{S_{i-1}}\right) + \frac{\left(\overline{S_{i+1}} - \overline{S_{i-1}}\right)}{\left(i-1\right)}\right] \tag{25}$$

- At the external surface (Z = 1, j = N)

$$\frac{d\overline{S_N}}{d\tau} = 2A\left(\overline{S_M}\right)\left[\left(\frac{\Delta Z\mathrm{Bi}\left(\overline{S_{\mathrm{bt}}} - \overline{S_M}\right) + \overline{S_{M-1}} - \overline{S_M}}{\Delta Z^2}\right) + \frac{\mathrm{Bi}\left(\overline{S_{\mathrm{bt}}} - \overline{S_M}\right)}{\left(M-1\right)\Delta Z}\right] \tag{26}$$

External film resistance model is valid only if the contacting time between the liquid and solid phases is less than 25 min. In the later stages of adsorption, internal pore diffusion plays a vital role than external mass transfer effects. Based upon this, most of the models were described with internal pore diffusivity and external mass transfer co-efficient as a function of initial dye solution concentration. In order to get accurate mass transfer parameter namely diffusivity and mass transfer co-efficient, film-pore diffusion model has been suggested. Diffusivity and mass transfer coefficient were determined by Excel 2003 solver, Eqs. (24)–(26). The film-pore diffusion model was solved by Microsoft Excel 2003. Solver-add in (Microsoft Excel 2003) was employed in order to determine the appropriate values of external mass transfer co-efficient and internal pore diffusivity that could minimize the error function described earlier.

The input to the program namely (1) average size of the particle, (2) dosage, (3) initial dye concentration, (4) Langmuir adsorption isotherm kinetic parameters, (5) number of grid points used in radial coordinate and (6) number of time steps were applied. The internal pore diffusivity and external mass transfer co-efficient from single resistance model has been considered as initial guess to execute the program. The values of internal effective diffusivity and external mass transfer co-efficient were iterated with solver add-in (Excel 2003) till the summation of Chi-square, χ^2, values minimized. It was known that film-pore diffusion model was suitable to explain MB concentration decay curve and it is also possible to obtain a single value of k_s and D_{eff} for

Table 1
Effect of initial dye concentration on pseudo-second-order kinetic parameters for the adsorption of MB on ASB (dosage = 5 g dm^{-3}, agitation speed = 100 rpm, particle size: BSS ≠ –14 + 36)

Dye concentration, mg dm^{-3}	Temperature °C	$Q_{e,\mathrm{exp}}$ (mg g^{-1})	k_2, g mg^{-1} min^{-1}	$Q_{e,\mathrm{pre}}$ (mg g^{-1})	h (mg g^{-1} min^{-1})	Chi-square error
50	25	8.36	0.791	8.196	53.19	0.97
	30	8.16	0.96	8.4	67.56	
	40	7.56	0.42	7.692	24.94	
	50	6.6	0.27	6.849	12.67	
100	25	15.4	0.35	13.51	64.52	0.08
	30	13.4	0.257	15.63	62.89	
	40	11.6	0.172	12.048	24.93	
	50	9.6	0.068	10.53	7.53	
150	25	22.2	0.051	22.22	25.19	0.06
	30	21.0	0.121	22.73	62.5	
	40	19.2	0.089	20.0	35.59	
	50	19.8	0.087	16.7	24.17	
200	25	31.2	0.189	33.3	21.01	0.03
	30	30.4	0.326	33.3	36.23	
	40	25.4	0.04	27.027	29.24	
	50	24.2	0.049	21.28	22.18	
250	25	36.2	0.0383	37.037	52.63	0.56
	30	35.0	0.071	37.037	97.08	
	40	31.0	0.046	32.26	48.78	
	50	25.0	0.066	24.2	38.65	

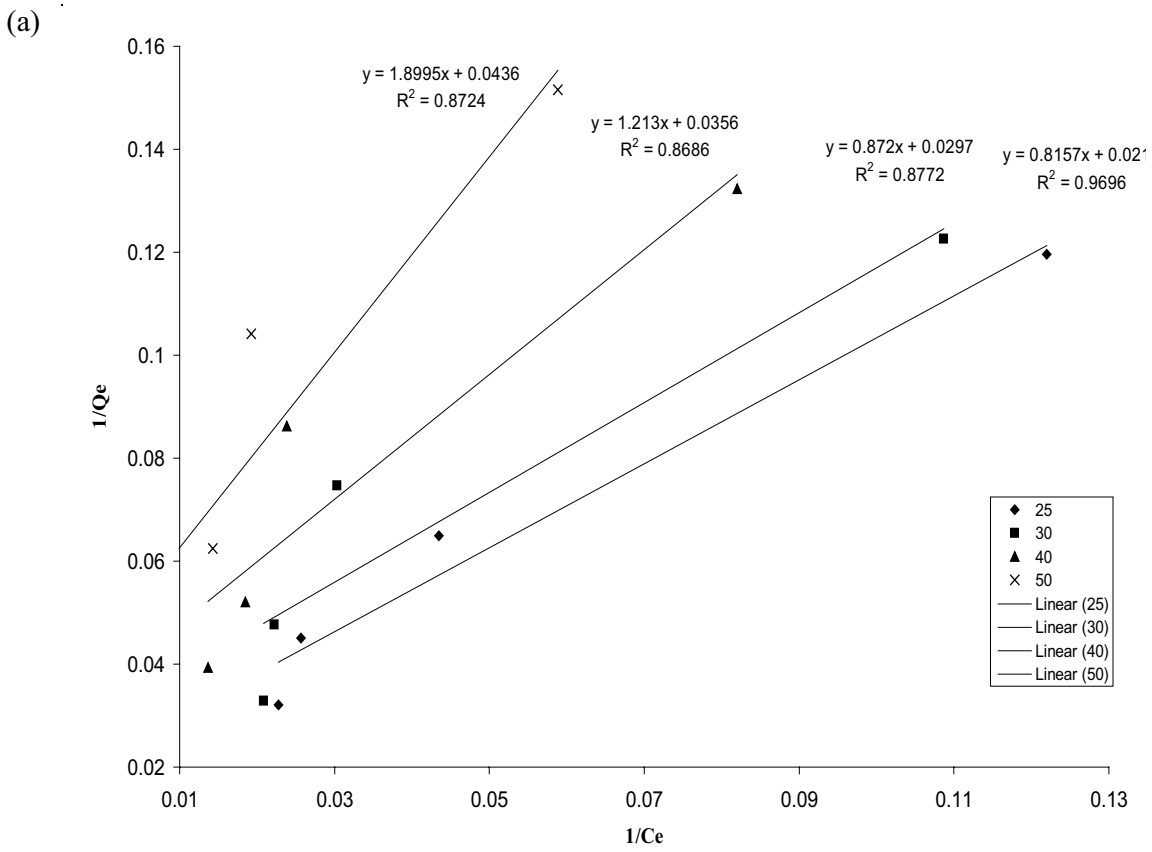

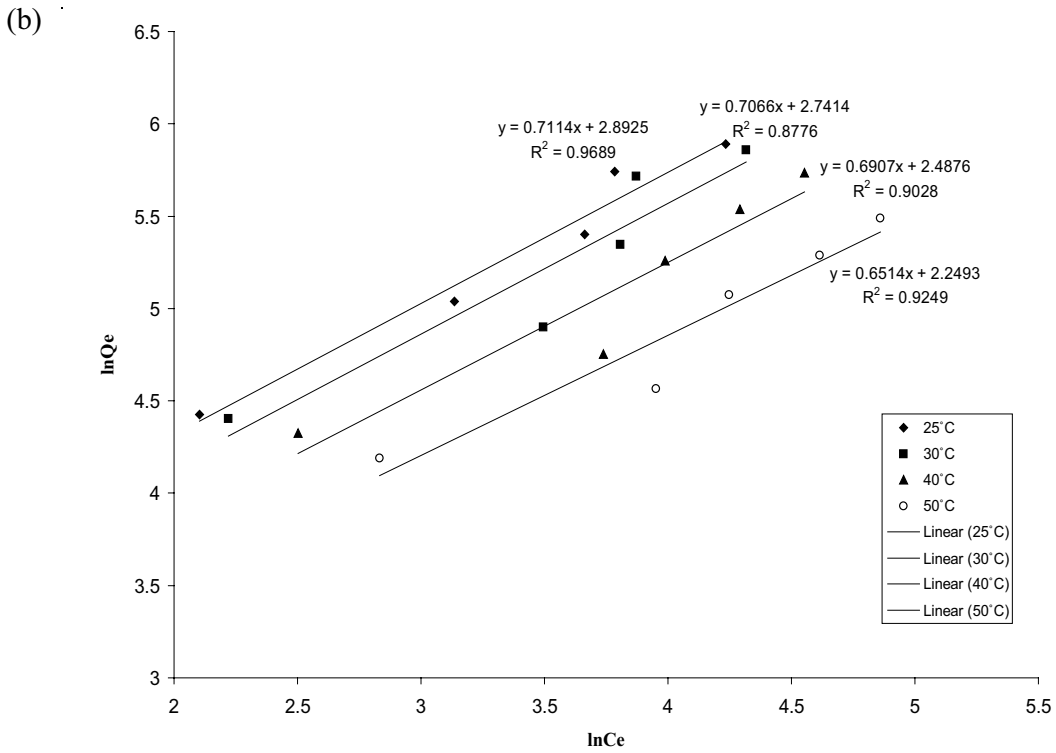

Fig. 8. Biosorption isotherm models using ASB (a) Langmuir biosorption model and (b) Freundlich biosorption model (dosage = 5 g dm^{-3}, agitation speed = 100 rpm; particle size: BSS ≠ –14 + 36).

Table 2
Determination of equilibrium parameters for adsorption of MB dye on ASB (dosage = 5 g dm^{-3}, agitation speed = 100 rpm; particle size: BSS ≠ –14 + 36)

Temperature, °C	Langmuir			Freundlich		
	Q_m, mg g^{-1}	K, dm^3 mg^{-1}	R^2	K_F (mg g^{-1}) (dm^3 mg^{-1})$^{-1/n}$	N	R^2
25	45.4	0.025	0.9696	1.77	1.4	0.9689
30	33.3	0.026	0.8772	1.54	1.42	0.8776
40	27.7	0.023	0.8686	1.2	1.45	0.9028
50	27	0.018	0.8724	0.96	1.54	0.9249

Table 3
Comparison of monolayer maximum specific adsorption capacity

S. No	Adsorbent	Monolayer maximum specific adsorption capacity, mg g^{-1}	Reference
1.	Fly ash	120.48	[14]
2.	Attapulgite	100.2	[53]
3.	Saw dust	12.92	[16]
4.	Alkali-treated sun flower hill	169.5	[18]
5.	Jack fruit leaf powder	3.7	[21]
6.	Bengal gram fruit seed	22.2	[21]
7.	Rice husk	40.5	[42]
8.	Wheat shells	16.6	[4]
9.	Orange peel	18.6	[53]
10.	Cold plasma treated acorn shell	111.11	[54]
11.	Microwave radiation treated acorn shell	83.34	[54]
12.	Formaldehyde treated acorn shell	90.91	[54]
13.	ASB	45.9	This study

Table 4
Thermodynamics parameters for adsorption of MB on ASB (dosage = 5 g dm^{-3}, agitation speed = 100 rpm; particle size: BSS ≠ –14 + 36)

Temperature, °C	Q_m, mg g^{-1}	K	ln$K$	ΔG (kJ mol^{-1})	ΔH (kJ mol^{-1})	ΔS (J mol^{-1} K^{-1})	R^2
25	45.4	0.025	5.713733	–	–	–	–
30	33.3	0.026	5.746203	9.13			
40	27.7	0.023	5.777652	9.93	–14.9	–79.32	0.9572
50	27.0	0.018	5.808142	10.73			

all the concentrations using this film-pore diffusion model. The experimental data are well in agreement with predicted data for the adsorption of dye solution on ASB at 25°C. At high concentration of dye solution ranging from 150 to 250 mg dm^{-3}, the experimental data are slightly deviated from predicted data. This may be possible when the overall mass transfer is controlled by surface diffusion. Therefore, film-pore diffusion model is an appropriate one to describe the decay data of dye solution, determine mass transfer parameters namely internal pore diffusivity and external mass transfer coefficient at a given temperature. The overall rate is controlled by film diffusion when liquid film diffusivity is ranging from 10^{-6} to 10^{-8} cm^2 s^{-1}. However, internal pore diffusion is predominant due to the larger value of Biot number [29,54]. And also, the increase in temperature of the system increases the external mass transfer co-efficient due to greater motion of dye molecules and decrease in effective film thickness [29]. The effective pore diffusivity is greatly influenced by physico-chemical properties of diffusing dye solute namely polarity, size and solubility. The pore diffusivity is smaller due to larger molecular weight of Methylene Blue dye. In this study, external mass transfer co-efficient (k_s) and internal effective diffusivity (D_{eff}) are ranging from 10^{-6} to 10^{-12} m^2 s^{-1} as given in Table 5. The findings were consistent with previous reports [29,54]. Therefore, internal pore diffusion is the rate-controlling step for adsorption of dye solution on ASB due to large value of Biot number. As temperature increases, the value of Biot number is decreased.

Table 5
Determination of internal effective diffusivity and external mass transfer coefficient at 298 K (dosage = 5 g dm^{-3}, agitation speed = 100 rpm; particle size: BSS ≠ –14 + 36)

Temperature, °C	Initial dye concentration (S_i), mg L^{-1}	*ks*, m s^{-1}	D_e, m^2 s^{-1}	Bi
30	50 100 150 200 250	5.01×10^{-6}	3.03×10^{-12}	1,112.11
40	50 100 150 200 250	5.03×10^{-6}	2.4×10^{-12}	222.42
50	50 100 150 200 250	6.5×10^{-5}	1.32×10^{-12}	44.48

4. Conclusion

- Influence of quantity of adsorbent, initial pH, initial composition of dye solution and temperature on specific dye uptake was investigated. The maximum adsorption capacity was improved to 45.4 mg g^{-1} at 298 K using ASB.
- The adsorption shows a decreasing trend with respect to increase in temperature. Therefore, adsorption is exothermic. Moreover, the positive Gibbs free energy change and negative entropy change describe that the sorption is not favorable at temperature more than 30°C.
- The film pore diffusion model was applied to explain the decay rate of dye solution on ASB. The experimental decay data are well in agreement with predicted data other than high concentration of dye solution. Based on the results, it is concluded that ASB can be a cost-effective and potential adsorbent and can be employed for decolorization of industrial textile dye effluent also.

Acknowledgment

The authors are thankful to their management (SASTRA Deemed University) who provided the facilities that greatly supported the research work.

Symbols

A_s — Total surface area of all the adsorbent, m^2 dm^{-3}
Bi — Biot number, dimensionless
S — Bulk composition of MB, mg dm^{-3}
C_e — Equilibrium MB composition in liquid phase, mg dm^{-3}
S_0 — Initial MB composition in bulk solution, mg dm^{-3}
S_s — Surface concentration, mg dm^{-3}
D — Adsorbent dose, g dm^{-3}
D_e — Internal effective diffusivity, m^2 s^{-1}
D_p — Internal diffusivity, m^2 s^{-1}
d_p — Diameter of particle, m
K_2 — Pseudo-second-order rate constant, g mg^{-1} min^{-1}
k_f — External film transfer coefficient, m s^{-1}
K_F — Freundlich constant, g^{-1} dm^3 $mg^{1-1/n}$
K_L — Langmuir adsorption constant, dm^3 mg^{-1}
M_s — Mass of particles added, g dm^{-3}
n — Freundlich parameter
Q_e — Solid-phase dye concentration at equilibrium, mg g^{-1}
Q_m — Maximum dye adsorbed per unit mass of adsorbent (mono layer capacity), mg g^{-1}
Q_t — Solid-phase dye concentration at time t, mg g^{-1}
R^2 — Coefficient of determination
R_L — Langmuir separation or equilibrium parameter, dimensionless
Sh — Sherwood number
t — Time, s or min
T — Absolute temperature, K
V_L — Volume of solution, dm^3
ΔG — Free energy of adsorption, kJ mol^{-1}
ΔH — Change in enthalpy, kJ mol^{-1}
ΔS — Change in entropy, kJ mol^{-1} K^{-1}

References

[1] P. Saha, S. Datta, Assessment on thermodynamics and kinetics parameters on reduction of methylene blue dye using flyash, Desal. Wat. Treat., 12 (2009) 219–228.
[2] M.K. Dahri, M.R.R. Kooh, L.B.L. Lim, Application of *Casuarina equisetifolia* needle for the removal of methylene blue and malachite green dyes from aqueous solution, Alexandria Eng. J., 54 (2015) 1253–1263.
[3] M. Rafatullah, O. Sulaiman, R. Hashim, A. Ahmad, Adsorption of methylene blue on low-cost adsorbents: a review, J. Hazard. Mater., 177 (2010) 70–80.

[4] Y. Bulut, H. Aydın, A kinetics and thermodynamics study of methylene blue adsorption on wheat shells, Desalination, 194 (2006) 259–267.
[5] A.R. Khataee, F. Vafaei, M. Jannatkhah, Biosorption of three textile dyes from contaminated water by filamentous green algal *Spirogyra* sp.: kinetic, isotherm and thermodynamic studies, Int. Biodeterior. Biodegrad., 83 (2013) 33–40.
[6] N.E. Messaoudi, M.E. Khomri, A. Dbik, S. Bentahar, A. Lacherai, B. Bakiz, Biosorption of Congo red in a fixed-bed column from aqueous solution using jujube shell: experimental and mathematical modeling, J. Environ. Chem. Eng., 4 (2016) 3848–3855.
[7] S. Rangabhashiyam, S. Lata, P. Balasubramanian, Biosorption characteristics of methylene blue and malachite green from simulated wastewater onto *Carica papaya* wood biosorbent, Surf. Interfaces, 10 (2018) 197–215.
[8] S. Rangabhashiyam, N. Anu, N. Selvaraju, Sequestration of dye from textile industry wastewater using agricultural waste products as adsorbents, J. Environ. Chem. Eng., 1 (2013) 629–641.
[9] M.E. Haddad, A. Regti, R. Slimani, S. Lazar, Assessment of the biosorption kinetic and thermodynamic for the removal of safranin dye from aqueous solutions using calcined mussel shells, J. Ind. Eng. Chem., 20 (2014) 717–724.
[10] A. Abdolali, W.S. Guo, H.H. Ngo, S.S. Chen, N.C. Nguyen, K.L. Tung, Typical lignocellulosic wastes and by-products for biosorption process in water and wastewater treatment: a critical review, Bioresour. Technol., 160 (2014) 57–66.
[11] S. Rangabhashiyam, E. Suganya, N. Selvaraju, L.A. Varghese, Significance of exploiting non-living biomaterials for the biosorption of wastewater pollutants, World J. Microbiol. Biotechnol., 30 (2014) 1669–1689.
[12] K. Vijayaraghavan, S. Rangabhashiyam, T. Ashokkumar, J. Arockiaraj, Assessment of samarium biosorption from aqueous solution by brown macroalga *Turbinaria conoides*, J. Taiwan Inst. Chem. Eng., 74 (2017) 113–120.
[13] S.M.H. Gardazi, T.A. Butt, N. Rashid, A. Pervez, Q. Mahmood, M.M. Shah, M. Bilal, Effective adsorption of cationic dye from aqueous solution using low-cost corncob in batch and column studies, Desal. Wat. Treat., 57 (2016) 28981–28998.
[14] S. Agarwal, S. Yadav, A. Sharma, K. Singh, A.B. Gupta, Kinetic and equilibrium studies of decolorization of effluent of handmade paper industry by low-cost fly ash, Desal. Wat. Treat., 57 (2016) 25783–25799.
[15] N. Saadon, N. Razali, M.M. Yashim, N.A. Yusof, Adsorption of methylene blue using oil palm (*Elaeis Guaneensis*) fronds as activated carbon, ARPN J. Eng. Appl. Sci., 9 (2016) 6191–6194.
[16] A. Najafpoor, H. Alidadi, H. Esmaeili, T. Hadilou, M. Dolatabadi, A. Hosseinzadeh, M. Davoudi, Optimization of anionic dye adsorption onto *Melia azedarach* sawdust in aqueous solutions: effect of calcium cations, Asia-Pac. J. Chem. Eng., 2 (2016) 258–270.
[17] K. Simarani, M.N. Saat, M.S.M. Annuar, Efficient removal of azo dye by grated copra biomass, Desal. Wat. Treat., 57 (2016) 230–237.
[18] G.B. Oguntimein, Biosorption of dye from textile wastewater effluent onto alkali treated dried sunflower seed hull and design of a batch adsorber, J. Environ. Chem. Eng., 4 (2015) 2647–2661.
[19] A. Geetha, P.N. Palanisamy, Application of activated carbon and polypyrrole coated sawdust for adsorption of acidic dye from aqueous solutions: a comparative study, Asian J. Chem., 8 (2015) 2813–2818.
[20] C. Umpuch, Removal of yellow 20 dye from aqueous solution using organo-rice straw: characteristic, kinetic and equilibrium studies, Eng. J., 2 (2015) 59–69.
[21] A.K. Ojha, V.K. Bulasara, Adsorption characteristics of jackfruit leaf powder for the removal of Amido black 10B dye, Environ. Prog. Sustainable Energy, 2 (2015) 461–470.
[22] L. Sivarama Krishna, A. Sreenath Reddy, A. Muralikrishna, W.Y. Wan Zuhairi, H. Osman, A. Varada Reddy, Utilization of the agricultural waste (*Cicer arientinum Linn* fruit shell biomass) as biosorbent for decolorization of Congo red, Desal. Wat. Treat., 56 (2015) 2181–2192.
[23] Q. Li, S. Zhou, F. Li, Y. Yang, Adsorptive properties of municipal solid waste incinerator fly ash after different treatments to methylene blue, Chin. J. Environ. Eng., 9 (2015) 367–373.
[24] N.A. Fathy, O.I. El-Shafey, L.B. Khalil, Effectiveness of alkali-acid treatment in enhancement the adsorption capacity for rice straw: the removal of methylene blue dye, ISRN Phys. Chem., 2013 (2013) 15 p, http://dx.doi.org/10.1155/2013/208087.
[25] J.O. Amode, J.H. Santos, Z.M. Alam, A.H. Mirza, C.C. Mei, Adsorption of methylene blue from aqueous solution using untreated and treated (*Metroxylon* spp.) waste adsorbent: equilibrium and kinetics studies, Int. J. Ind. Chem., 7 (2016) 333–345.
[26] A.A. Kadam, H.S. Lade, S.M. Patil, S.P. Govindwar, Low cost $CaCl_2$ pretreatment of sugarcane bagasse for enhancement of textile dyes adsorption and subsequent biodegradation of adsorbed dyes under solid state fermentation, Bioresour. Technol., 132 (2013) 276–284.
[27] G. Mckay, B. Al-Duri, Study of the mechanism of pore diffusion in batch adsorption systems, J. Chem. Technol. Biotechnol., 48 (1990) 269–285.
[28] B. Al Duri, G. Mckay, Basic dye adsorption on carbon using a solid-phase diffusion model, Chem. Eng. J., 38 (1988) 23–32.
[29] V. Ponnusami, K.S. Rajan, S. Srivastava, Application of film-pore diffusion model for methylene blue adsorption onto plant leaf powders, Chem. Eng. J., 163 (2010) 236–242.
[30] Y. Önal, B. Akmil-Başar, Ç. Sarıcı-Özdemir, Investigation kinetics mechanisms of adsorption malachite green onto activated carbon, J. Hazard. Mater., 146 (2007) 194–203.
[31] R.L. Zorica, D.S. Mirjana, B.M. Smilja, V.M. Jelena, L.M. Marija, S.K.R. Tatjana, L.J.K. Mirjana, Effects of different mechanical treatments on structural changes of lignocellulosic waste biomass and subsequent Cu(II) removal kinetics, Arabian J. Chem., (2016), (In Press), https://doi.org/10.1016/j.arabjc.2016.04.005.
[32] S. Rangabhashiyam, N. Selvaraju, Adsorptive remediation of hexavalent chromium from synthetic wastewater by a natural and $ZnCl_2$ activated *Sterculia guttata* shell, J. Mol. Liq., 207 (2015) 39–49.
[33] T. Akar, B. Anilan, A. Gorgulu, S.T. Akar, Assessment of cationic dye biosorption characteristics of untreated and non-conventional biomass: *Pyracantha coccinea* berries, J. Hazard. Mater., 168 (2009) 1302–1309.
[34] A.M. Aljeboree, A.N. Alshirifi, A.F. Alkaim, Kinetics and equilibrium study for the adsorption of textile dyes on coconut shell activated carbon, Arabian J. Chem., 10 (2017) S3381–S3393.
[35] K.S. Hameed, P. Muthirulan, S.M. Meenakshi, Adsorption of chromotrope dye onto activated carbons obtained from the seeds of various plants: equilibrium and kinetics studies, Arabian J. Chem., 10 (2017) S2225–S2233.
[36] R. Malik, D.S. Ramteke, S.R. Wate, Adsorption of malachite green on groundnut shell waste based powdered activated carbon, Waste Manage., 27 (2007) 1129–1138.
[37] K.V. Kumar, A. Kumaran, Removal of Methylene blue by Mango seed kernel powder, Biochem. Eng. J., 27 (2005) 83–93.
[38] N. Ahalya, M.N. Chandraprabha, R.D. Kanamadi, T.V. Ramachandra, Adsorption of methylene blue and amaranth on to tamarind pod shells, J. Biochem. Technol., 3 (2012) S189–S192.
[39] N.F. Cardoso, E.C. Lima, B. Royer, M.V. Bach, G.L. Dotto, L.A.A. Pinto, T. Calvete, Comparison of *Spirulina platensis* microalgae and commercial activated carbon as adsorbents for the removal of reactive Red 120 dye from aqueous effluents, J. Hazard. Mater., 241–242 (2012) 146–153.
[40] V. Ponnusami, S.N. Srivastava, Studies on application of teak leaf powders for the removal of color from synthetic and industrial effluents, J. Hazard. Mater., 169 (2009) 1159–1162.
[41] K.V. Kumar, K. Porkodi, Mass transfer, kinetics and equilibrium studies for the biosorption of methylene blue using *Paspalum notatum*, J. Hazard. Mater., 146 (2007) 214–226.
[42] V. Vadivelan, K.V. Kumar, Equilibrium, kinetics, mechanism, and process design for the sorption of methylene blue onto rice husk, J. Colloid Interface Sci., 286 (2005) 90–100.
[43] P. Velmurugan, V. Rathina Kumar, G. Dhinakaran, Dye removal from aqueous solution using low cost adsorbent, Int. J. Environ. Sci., 1 (2011) 1492–1503.

[44] V.S. Mane, I.D. Mall, V.C. Srivastava, Use of bagasse fly ash as an adsorbent for the removal of brilliant green dye from aqueous solution, Dyes Pigm., 73 (2007) 269–278.
[45] A. Fegousse, A. El Gaidoumi, Y. Miyah, R. El Mountassir, A. Lahrichi, Pineapple bark performance in dyes adsorption: optimization by the central composite design, J. Chem., 2019 (2019) 11 p, https://doi.org/10.1155/2019/3017163.
[46] R. Tang, C. Dai, C. Li, W. Liu, S. Gao, C. Wang, Removal of Methylene Blue from aqueous solution using agricultural residue walnut shell: equilibrium, kinetic, and thermodynamic studies, J. Chem., 2017 (2017) 10 p, https://doi.org/10.1155/2017/8404965.
[47] S. Kumar, A. Singh Ahluwalia, M.U. Charaya, Adsorption of Orange-G dye by the dried powdered biomass of *Chlorella vulgaris* Beijerinck, Curr. Sci., 116 (2019) 604–611.
[48] M.E. Mahmoud, M.M. Osman, S.B. Ahmed, T.M. Abdel-Fattah, Enhanced removal of lead by chemically and biologically treated carbonaceous materials, Sci. World J., 2012 (2012) 11 p, doi:10.1100/2012/604198.
[49] B.H. Hameed, F.B.M. Daud, Adsorption studies of basic dye on activated carbon derived from agricultural waste: *Hevea brasiliensis* seed coat, Chem. Eng. J., 139 (2008) 48–55.
[50] M.I. El-Khaiary, Kinetics and mechanism of adsorption of methylene blue from aqueous solution by nitric-acid treated water-hyacinth, J. Hazard. Mater., 147 (2007) 28–36.
[51] A.E. Ofomaja, Y.-S. Ho, Equilibrium sorption of anionic dye from aqueous solution by palm kernel fibre as sorbent, Dyes Pigm., 74 (2007) 60–66.
[52] K.M. Doke, E.M. Khan, Equilibrium, kinetic and diffusion mechanism of Cr(VI) adsorption onto activated carbon derived from wood apple shell, Arabian J. Chem., 10 (2017) 252–260.
[53] G. Annadurai, R.-S. Juang, D.-J. Lee, Use of cellulose-based wastes for adsorption of dyes from aqueous solutions, J. Hazard. Mater., 92 (2002) 263–274.
[54] C. Saka, Ö. Şahin, H. Adsoy, Ş.M. Akyel, Removal of Methylene Blue from aqueous solutions by using cold plasma, microwave radiation and formaldehyde treated acorn shell, Sep. Sci. Technol., 10 (2012) 1542–1551.